

From the Department of Medical Biochemistry and Biophysics  
Karolinska Institutet, Stockholm, Sweden

# **DECIPHERING EPHRIN/EPH SIGNALING PATHWAYS IN CANCER CELLS USING RATIONALLY DESIGNED LIGAND NANOCLUSTERS**

Alan Shaw



**Karolinska  
Institutet**

Stockholm 2017

All previously published papers were reproduced with permission from the publisher.

Published by Karolinska Institutet.

Printed by Eprint AB

© Alan Shaw, 2017

ISBN 978-91-7676-540-1

# DECIPHERING EPHRIN/EPH SIGNALING PATHWAYS IN CANCER CELLS USING RATIONALLY DESIGNED LIGAND NANOCCLUSERS

## THESIS FOR DOCTORAL DEGREE (Ph.D.)

By

**Alan Shaw**

*Principal Supervisor:*

Associate Professor Björn Högberg  
Karolinska Institutet  
Department of Medical Biochemistry and  
Biophysics  
Division of Biomaterials and Regenerative  
Medicine

*Co-supervisors:*

Associate Professor Ana Teixeira  
Karolinska Institutet  
Department of Medical Biochemistry and  
Biophysics  
Division of Biomaterials and Regenerative  
Medicine

Dr. Andreas Nyström  
Naturvetarna

*Mentor:*

Professor Adolf Gogoll  
Uppsala University  
Department of Biochemistry and Organic  
Chemistry

*Opponent:*

Professor Kurt Vesterager Gothelf  
Aarhus University  
Department of Chemistry

*Examination Board:*

Professor Mats Nilsson  
Stockholm University  
Department of Biochemistry and Biophysics

Professor Edvard Smith  
Karolinska Institutet  
Department of Laboratory Medicine

Professor Jussi Taipale  
Karolinska Institutet  
Department of Medical Biochemistry and  
Biophysics  
Division of Functional Genomics





To My Family and Friends



## **ABSTRACT**

The dynamic link between the nanoscale spatial distribution of biomolecules and their functional impact on cellular and downstream biological behaviors has been hypothesized, but only supported by limited evidences. This is mostly due to the lack to methods to fabricate well-defined patterns of biomolecules. In this thesis, we utilized the DNA origami method to create protein ligand and antigen patterns with high precision, and applied it to study cell signaling events in a cancer cell line and complex antibody-antigen interactions. In addition, to achieve quality fabrication of our protein and antigen functionalized DNA origami nanostructures we developed and adapted several DNA and protein purification methods. Finally, we employed the versatility of the DNA origami method to create anti-cancer drug carriers with tunable drug release kinetics.

## LIST OF SCIENTIFIC PAPERS

- I. Shaw, A.; Lundin, V.; Petrova, E.; Fördös, F.; Benson, E.; Al-Amin, A.; Herland, A.; Blokzijl, A.; Högberg, B.; Teixeira, A. I. Spatial Control of Membrane Receptor Function Using Ligand Nanocalipers. *Nat. Methods* **2014**, 11, 841–846.
- II. Shaw, A.; Högberg, B. Resolving Peculiar Antibody-Antigen Interactions with Patterned Surface Plasmon Resonance. *Manuscript*.
- III. Shaw, A.; Benson, E.; Högberg, B. Purification of Functionalized DNA Origami Nanostructures. *ACS Nano* **2015**, 9, 4968–4975.
- IV. Zhao, Y.-X.; Shaw, A.; Zeng, X.; Benson, E.; Nyström, A. M.; Högberg, B. DNA Origami Delivery System for Cancer Therapy with Tunable Release Properties. *ACS Nano* **2012**, 6, 8684–8691.

# CONTENTS

1	Introduction .....	1
1.1	The DNA origami method .....	1
1.2	Bioorthogonal click chemistry and bioconjugation.....	2
1.3	Ephrin and Eph .....	5
1.4	The flexibility and binding patterns of antibodies.....	6
1.5	Production and purification of functionalized DNA origami .....	8
1.6	DNA origami as drug delivery vessels .....	9
2	Materials and Methods .....	10
2.1	Design and fabrication of DNA origami nanostructures.....	10
2.1.1	caDNA <sup>no</sup> .....	10
2.1.2	Fabrication the DNA origami nanostructures .....	10
2.1.3	Bioconjugation between proteins and oligonucleotide handles.....	11
2.1.4	Functionalization of DNA origami nanostructures .....	13
2.1.5	Purification of the functionalized DNA origami nanostructures .....	13
2.2	Studying binding kinetics with surface plasmon resonance .....	14
2.2.1	Ephrin-A5-Fc and EphA2 binding kinetics.....	14
2.2.2	Antibody binding kinetics.....	14
2.3	Cellular signaling experiments.....	15
2.3.1	Cell culture and Eph receptor stimulation .....	15
2.3.2	Cell invasion assay .....	16
3	Results and Discussion.....	17
3.1.1	Folding and functionalization of DNA origami nanostructures (Paper I) .....	17
3.1.2	Characterization of the bio-availability of ephrin-A5-Fc nanocalipers (Paper I) .....	19
3.1.3	Spatial regulation of EphA2 receptor activation (Paper I).....	21
3.1.4	Studying antibody flexibility and complex antigen binding with PSPR (Paper II) .....	23
3.1.5	Purification of functionalized DNA origami nanostructures (Paper III) .....	25
3.1.6	DNA origami drug delivery system with tunable release properties (Paper IV) .....	29
4	Acknowledgements .....	33
5	References .....	34

## LIST OF ABBREVIATIONS

DNA	Deoxyribonucleic acid
A	Adenine
T	Thymine
G	Guanine
C	Cytosine
18HB	18 helix bundle
AFM	Atomic force microscopy
DBCO	Dibenzocyclooctyne
NHS	N-Hydroxysuccinimide
EDC	1-Ethyl-3-(3-dimethylaminopropyl)carbodiimide
DOX	Doxorubicin
SPR	Surface plasmon resonance
Da	Dalton
Eph	erythropoietin-producing human hepatocellular receptors
Ephrin	Eph family receptor interacting proteins
FACS	Fluorescence-activated cell sorting
nm	nanometer
FPLC	Fast protein liquid chromatography
TEM	Transmission electron microscopy
JR	DNA origami rectangular hollow brick
s.e.m.	Standard error

# 1 INTRODUCTION

## 1.1 THE DNA ORIGAMI METHOD

Deoxyribonucleic acid (DNA) is the biomolecule that stores genetic information essential to maintain and reproduce life. Using its four unique bases, Adenine (A), Thymine (T), Cytosine (C) and Guanine (G) as building blocks, it is possible to generate virtually unlimited combinations of DNA sequences, hence a massive amount of biological information can be stored within. According to the complementary base pairing rule, A can form two stable hydrogen bonds with T, and C can form three stable hydrogen bonds with G (Figure 1a). Two DNA strands that are complementary to each other can interact and form a DNA double helix. However, the versatility and programmability of DNA is not limited to vast genetic information storage, it can also be engineered and applied to non-genetic applications.

In the 1980s, Prof. Nadrian Seeman demonstrated that by using a combination of partially complementary linear and circular oligonucleotides, it is possible to fabricate a nanoscale cube with DNA<sup>1</sup> (Figure 1b). This experiment established the field of DNA nanotechnology. In 2006, Paul Rothemund revolutionized the field of DNA nanotechnology by introducing the “scaffolded” DNA origami method<sup>2</sup>. He showed that by using a long ssDNA “scaffold” and hundreds of short synthetic “staple” oligonucleotides that are designed to hybridize to different sections on the scaffold, it is possible to “fold” the long ssDNA scaffold into virtually any nanoscale object with high yield (Figure 1c).

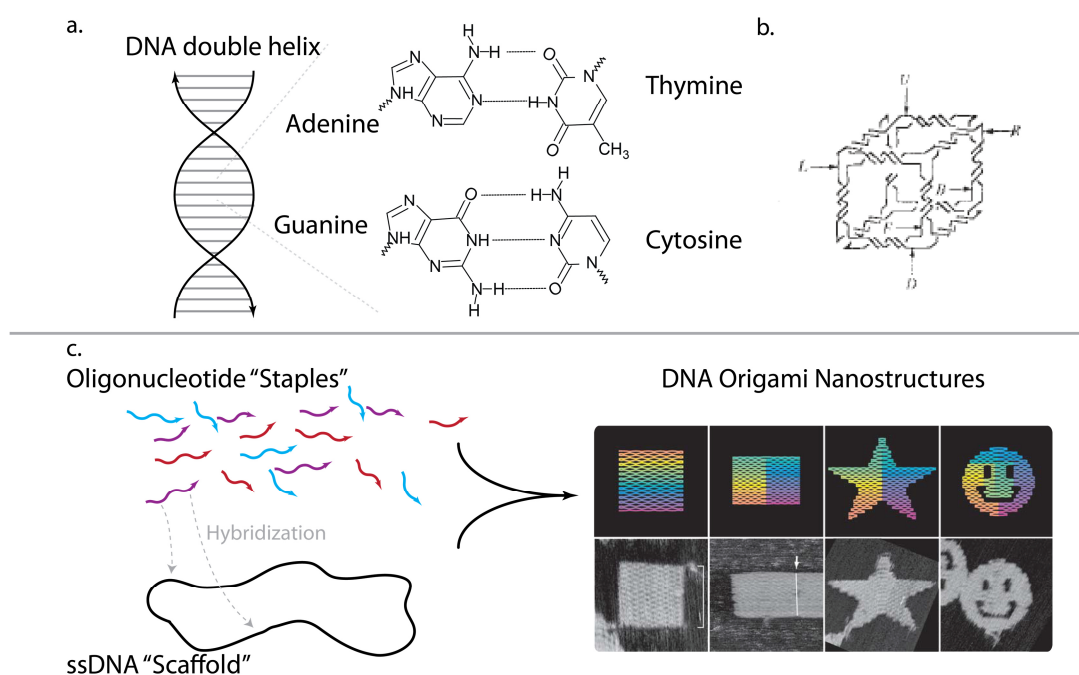


Figure 1. a. DNA double helixes are consisting of two complementary DNA chains. Adenine forms two hydrogen bonds with Thymine, Guanine forms three hydrogen bonds with Cytosine. b. The DNA nanocube synthesized by Professor Nadrian Seeman<sup>1</sup>. c. The DNA origami method developed by Paul Rothmund<sup>2</sup> (top right panel: computer rendering of the DNA nanostructures, bottom right panel: AFM micrographs of the DNA nanostructures, the boxes are 165 nm x 165 nm). b and the right panel of c was adapted with permission from nature publishing group.

The groundbreaking work of Nadrian Seeman and Paul Rothmund has ushered scientists into a new era of nanotechnology. With DNA nanotechnology and DNA origami, it is possible to designed and fabricate nano-scale objects from the bottom up with high fidelity. Using these promising tools to manipulate matter at the nanoscale, successful applications of DNA origami can be seen in the fields of chemistry<sup>3</sup>, structural<sup>4</sup> and cell biology<sup>5-7</sup>, drug delivery<sup>8,9</sup> and physics<sup>10</sup>.

In this thesis, we applied the DNA origami method to fabricate well-defined patterns of various biomolecules, and explored the fascinating interplay between the patterns, cellular behavior and immunological interactions.

## 1.2 BIOORTHOGONAL CLICK CHEMISTRY AND BIOCONJUGATION

One of the main challenges in the application of DNA origami is to decorate the origami nanostructures with various functional groups, such as proteins, chemicals and nanoparticles. Most common methods include: 1) incorporation of oligonucleotides that are directly modified with the functional group of interest (Figure 2, top panel). 2) incorporation of oligonucleotides modified with chemical linkers that can be further conjugated to the target functional group via click chemistry and 3) tagging of target functional group with a short handle oligonucleotide that can be further hybridized to a DNA origami that express the



complement oligo (Figure 2, bottom panel). All of these approaches require rapid and robust chemical reactions that are compatible with biological conditions to crosslink DNA with desired functional groups.

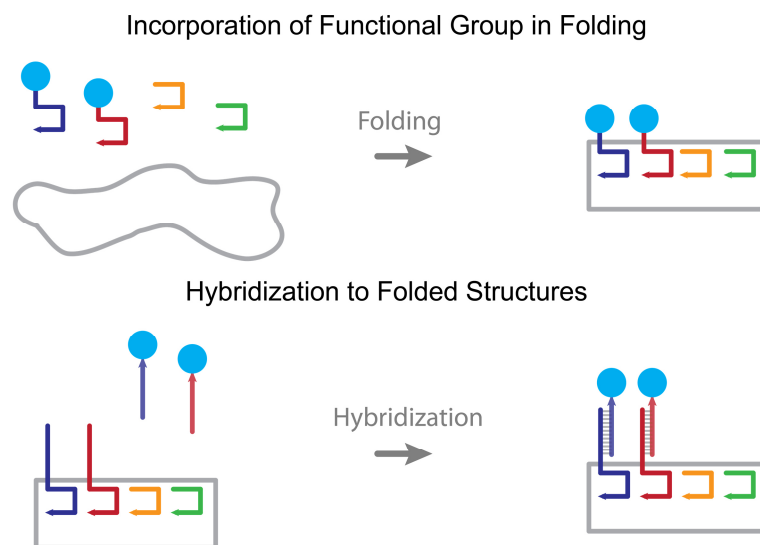


Figure 2. Different approaches to functionalize DNA origami nanostructures. Top panel: functional groups (blue circles) that are thermo-stable were directly incorporated in the folding process (color lines: staple oligonucleotides); Bottom panel: Heat sensitive functional groups such as the majority of proteins were conjugated first to a complementary handle oligonucleotide and then hybridized to folded nanostructures.

Click chemistry is a specific set of chemical reactions that are fast, specific and can be carried out in biological buffers. Since its first description in 2001 by Prof. Sharpless<sup>11</sup>, click chemistry has become one of the most important methods to tag biomolecules in a wide range of applications<sup>12</sup>. Some examples<sup>11</sup> of click chemistry include: hydrazone click chemistry, [3+2] cycloadditions, Diels-Alder reactions and [4+1] cycloadditions.

In this thesis, we applied NHS/EDC coupling, hydrazone chemistry and [3+2] cycloadditions to functionalize our DNA nanostructures (Figure 3). If we aim to functionalize our DNA origami nanostructures with proteins, we first modify both the protein of interest and the handle oligonucleotide with two different bifunctional linkers, and then cross link the two modified molecules with click chemistry (Figure 3 b and c). In the case of small molecule functionalization (such as haptens or fluorophores), we react amine modified oligos with the small molecules that are activated with NHS (Figure 3a), and incorporate the modified oligonucleotide in the folding process (Figure 2). We developed and adapted several protocols that are tailored to each type of functionalization we wish to achieve:

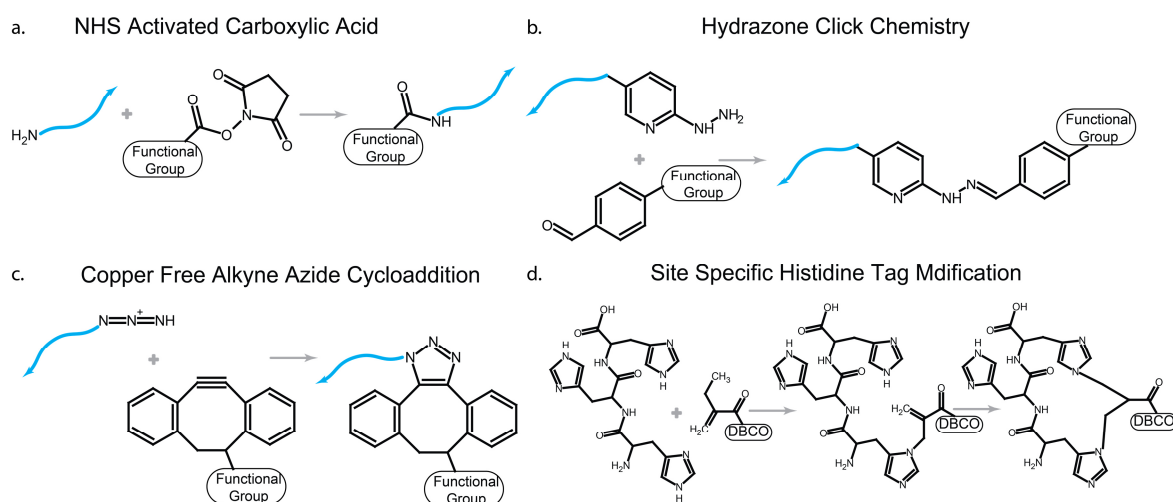


Figure 3. Different approaches in bio-conjugation. Blue line: amine modified oligonucleotide; DBCO: dibenzocyclooctyne; Functional Group: The functional molecule to be introduced to DNA origami.

### 1) NHS/EDC coupling (Figure 3a):

Small molecules that contain an NHS activated carboxylic acid can be reacted with amine modified oligonucleotides or accessible lysine residues on proteins. This is perhaps the most widely used method to tag biomolecules, and it is the first step in our preparation of our conjugates, but it suffers from several drawbacks: a) NHS activated carboxylic acids can be degraded by water, so in these type of reactions there is always a competition between amide bond formation and degradation, hence an excess of these NHS activated chemicals is often required. b) When tagging proteins, this technique targets any accessible lysine on the protein, so there is a risk to denature the protein if the tagging occurs at the binding or active site. Because of these reasons, care must be taken so we only obtain the minimum amount of tagging necessary to proceed with further conjugations.

### 2) Hydrazone click chemistry<sup>11</sup> (Figure 3b):

A hydrazine and an aldehyde can condense and form a hydrazone bond in mildly acidic conditions (pH6.0). By tagging proteins with hydrazine, and oligonucleotides with benzaldehyde, we can crosslink the two molecules. One of the advantages of this technique is the hydrazone bond produced has a unique absorbance of light at 350 nm and a known extinction coefficient, which makes the characterization of the conjugation yield easier. We can use the Bradford assay to measure the protein concentration, and the absorbance at 350 nm to estimate the hydrazone concentration, hence the conjugation yield can be quantified (ratio between the protein and the oligonucleotide).

### 3) Copper-free Alkyne-Azide [3+2] cycloaddition<sup>13</sup> (Figure 3c):

This reaction is modified from the well-known Huisgen 1,3-Dipolar Cycloaddition, which uses a copper catalysis to catalyze the cycloaddition between an alkyne and an azide, producing a triazole compound. The presence of copper can denature proteins and residues of

the metal can be cytotoxic. This drawback can be eliminated by using strained cyclic alkynes (such as cyclic-octyne). The alkyne group becomes much more reactive towards the azide due to its ring strain, and the cycloaddition can be carried in physiological conditions without the presence of copper.

4) Site specific tagging of the histidine tag with the bis-sulfone functional group<sup>14</sup> (Figure 3d):

To achieve site specific tagging of proteins, we adapted and developed this technique to “tag” and functionalize the histidine tag of proteins with cyclic-octyne, which can be further conjugated to an azide modified handle oligonucleotide. Lowering the pH of the reaction buffer to around 6.3, we will protonate the vast majority of accessible lysine residues on target protein, making them less nucleophilic, while the nucleophilic imidazole nitrogen on histidine remains unprotonated and nucleophilic. The bis-sulfone group then reacts with two histidines via two subsequent Michael additions, forming a heterocyclic 19 member ring, tagging the histidine tag site specifically with DBCO.

### 1.3 EPHRIN AND EPH

Membrane bound receptor-ligand interactions and their downstream signaling events regulate to a large extent the communication between cells<sup>15</sup>. In particular, the Eph receptors (erythropoietin-producing human hepatocellular receptors) are the largest known subfamily of receptor tyrosine kinases, and are activated upon binding with their membrane bound ephrin ligands. Eph-ephrin interactions were described to play critical roles in embryonic development, axon guidance and cell migration, and are often disrupted in various forms of cancer<sup>16</sup>. Considering the critical role of abnormal Eph-ephrin interactions in cancer, it is essential to understand their subtle signaling mechanisms in order to develop targeted therapeutics.

Studies have shown that Eph-ephrin interaction initiates further downstream signaling predominately via the formation of higher order receptor-ligand clusters that form at the cellular membrane<sup>17,18</sup> (Figure 4), and remains inactivated when the formation of such clusters is impeded<sup>19</sup>. The course of Eph receptor signaling has been classified into several steps: initiation of the signaling process by a single ephrin ligand-Eph receptor binding event or “seeding”; the seeding step is followed by hetero-tetramerization of two ephrin-Eph complexes and further recruitment of these complexes into higher order signaling clusters. This is supported by crystallography data<sup>17</sup>, which demonstrate that specific receptor-receptor, receptor-ligand interaction modes ensue the formation of receptor-ligand heterodimers, tetramers and oligomers.

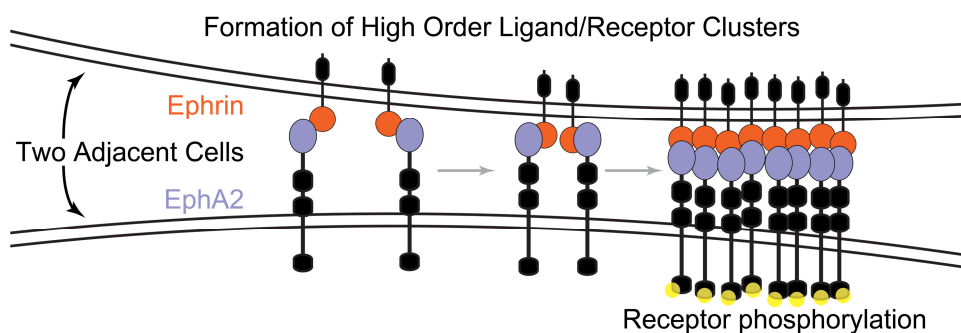


Figure 4. The proposed mechanism of ephrin/Eph clustering and signal transduction.

Membrane protein clustering events were hypothesized to function at the nanometer scale<sup>20</sup>. To probe the nanoscale mechanisms of Eph-ephrin interaction, we have chosen the DNA origami method<sup>2</sup> and developed a technique to present ephrin-A5-Fc ligands (a hybrid of ephrin-A5 and Fc that spontaneously forms dimers) at well-defined distances. Due to the ability of our DNA nanostructure to arrange ephrin-A5-Fc with high precision, we coin the term “ephrin-A5-Fc nanocalipers”. Using these ephrin-A5-Fc nanocalipers, we demonstrated that it is possible to induce ephrin-A5 distance-dependent EphA2 receptor activation and cellular behavior in a breast cancer cell line.

#### 1.4 THE FLEXIBILITY AND BINDING PATTERNS OF ANTIBODIES

Antibodies are one of the key components in the mammalian immune system; they were evolved to recognize and bind to antigens that are present on foreign organelles, and either physically block the protein-protein interactions required for the organelle’s survival and function, or act as a tag to initiate an attack from other components in the immune system. There are five classes of antibodies in the mammalian immune system, IgA, IgD, IgE, IgG and IgM, IgG performs the majority of antibody based immunity. IgG are large Y shaped proteins, with two antigen binding arms (Fab) and one stem region (Fc) that communicates with other components in the immune system. The two arms are joined together with the stem via a flexible hinge region to introduce flexibility to the molecule.

The flexibility of the antibody hinge region allows the two antigen binding arms to bind to wider ranges of antigen distances and orientations, which can translate into different immune responses<sup>21</sup>. Early studies showed that antibodies can form linear dimers, triangular trimers, and rectangular tetramers when multiple antibodies are crosslinked with dimers of small molecule antigens<sup>22</sup>. Recent transmission electron tomography studies revealed that the dynamic distance between the two Fab arms in human IgG1 is between 6 and 12 nanometers<sup>23</sup>. However, these studies are either based on imaging of fixed antibodies, or non-antigen bound antibodies, so precious kinetic and dynamic behaviors of the antibody-antigen interactions, with respect to the molecule’s flexibility are lost.

The assembly of antibody clusters subsequent to antigen binding on target organelle plays a critical role in the initiation of immune responses<sup>24</sup>. However, dynamics of detailed clustering interactions between multiple antigen and antibodies has not been described.

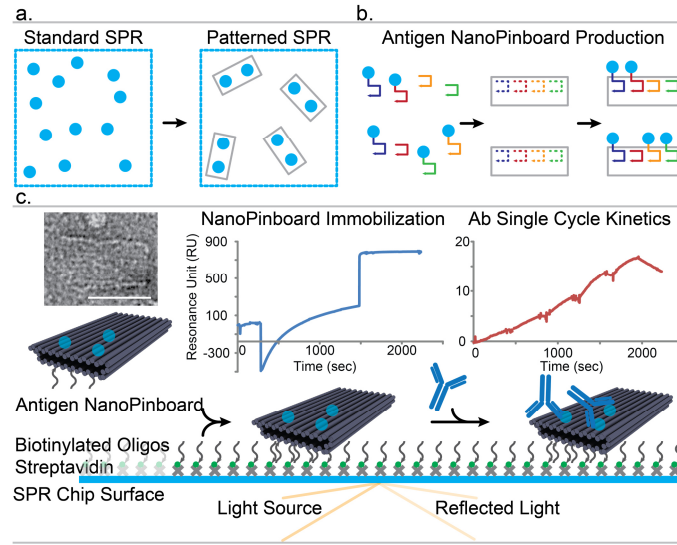


Figure 5. An overview of the patterned surface plasmon resonance (PSPR) method. a. In contrast to conventional SPR where the ligand of interest is randomly coupled to the surface, the PSPR method offers precise manipulation of ligand patterns on the surface. b. DNA origami antigen patterns were created by using different combinations of antigen modified staples. c. The antigen nanopinboards were immobilized on the SPR surface via oligonucleotide hybridization. An increasing concentration of antibodies was flown over the surface and binding interactions were recorded (scale bar for the TEM micrograph of the antigen nanopinboard: 50 nm, blue dots: antigens).

Surface plasmon resonance<sup>25</sup> is a technique that utilizes the changes in the absorbance of total internal reflected light when mass (such as proteins) are deposited on a gold surface. One of the binding partners, such as a receptor, is commonly immobilized on the gold surface via NHS/EDC coupling, and a concentration series of the ligand is flown through the surface. Once the ligands bind to the receptor, the mass on the surface increases, resulting in an increase in the SPR signal (resonance units), and recording the changes in SPR signal over time will result in a binding curve (a typical single cycle kinetics binding curve is shown in Figure 5c, top right panel). The binding curve is then fitted with a 1:1 Langmuir binding model to obtain the binding rates and constants.

Using DNA origami, we developed the patterned surface plasmon resonance (PSPR, Figure 5) technique, where we fabricate DNA nanopinboards to present antigens at different distances and patterns on an SPR surface (Figure 5c), and applied this method to study the interplay between the structures of the hinge region in different antibody subclasses and its binding kinetics to antigen dimers arranged at various distances. We also applied this technique to study the clustering interactions between multiple antibodies and antigens.

## 1.5 PRODUCTION AND PURIFICATION OF FUNCTIONALIZED DNA ORIGAMI

The DNA origami method has enabled the arrangement of matter and function at the nanoscale with high precision<sup>26</sup>. Oligonucleotides that control the folding of DNA origami structures can be modified with functional groups, and incorporated into the structures with high programmability. However, the realization of the functionalization process of these nanostructures can be tricky, in particular, the purification step that removes excess production materials from the functionalized DNA nanostructures. The functional groups are normally added in excess to the nanostructures to ensure good incorporation yield, but the presence of excess functionalization material can interfere and introduce errors in downstream applications. Hence robust methods to remove these excess materials are critical to obtain reliable experimental results. An additional complication arises when the functional groups, such as fluorophores and proteins, display unspecific interactions with membranes, resins and plastics<sup>27</sup>. These properties tend to render the functionalized structures stickier and an improper choice of purification method can result in poor recovery yield or poor purity.

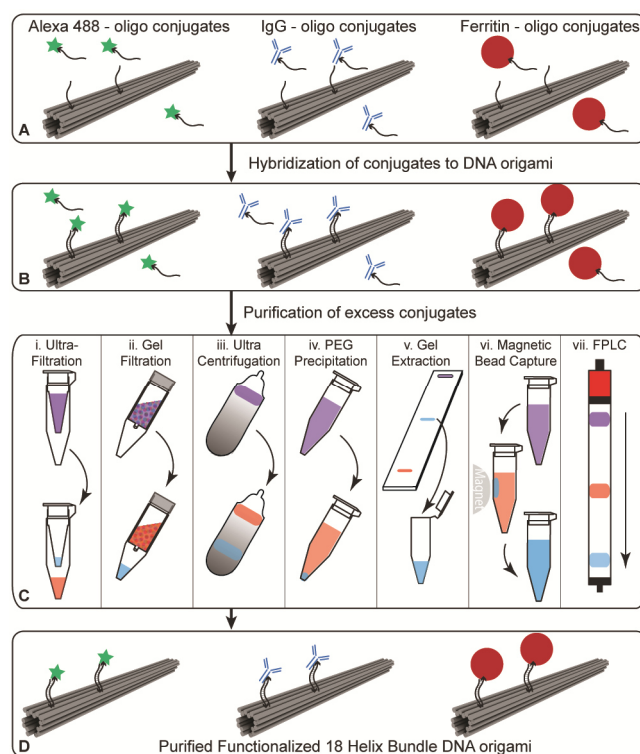


Figure 6. An overview of DNA origami functionalization and purification<sup>28</sup>. a and b. functional groups conjugated to the handle oligonucleotide were hybridized to the structures. c. excess functional groups were removed via the seven methods tested in this study. d. purified functionalized DNA origami were obtained.

A variety of methods exist for the purification of DNA or protein<sup>29</sup>, but these methods involve denaturing or breaking up the biomolecules other than the desired product. The purification of protein-decorated origami nanostructures requires the process to retain both the biological activity of the proteins, and the structural integrity of the nanostructures. Also,

most size-exclusion based methods are optimized to purify molecules in the kDa range, not supramolecular structures in the order of MDa. Because of these reasons, new and adapted methods have been developed to purify functionalized DNA origami structures, these methods include: poly-ethylene glycol fractionation<sup>30,31</sup>, gel extraction<sup>32</sup>, glycerol gradient ultracentrifugation<sup>33</sup>, size exclusion columns<sup>34</sup> and ultrafiltration<sup>5</sup> (Figure 6). But there is a lack of studies comparing the efficacy of these methods in a similar setup.

To compare the methods in a similar setup, we selected three functionalized DNA origami as model systems: Alexa488 modified DNA 18 helix bundle (A488-18HB), IgG modified DNA 18 helix bundle (IgG-18HB) and ferritin modified 18 helix bundle (ferritin-18HB). A488 represent purification of small molecules, IgG represents purification of moderate size (around 150 kDa) proteins and ferritin represents purification of large (around 500 kDa) proteins (Figure 6). We also demonstrated the efficacy of two adapted purification methods that have not been previously applied to purify DNA origami: Magnetic bead capture and size exclusion fast protein liquid chromatography.

## **1.6 DNA ORIGAMI AS DRUG DELIVERY VESSELS**

DNA origami nanostructures are highly programmable and can be easily functionalized with a plethora of functional groups<sup>5,6</sup>, these properties make the nanostructures a potential vessel to deliver and release drugs with high specificity. DNA origami has been successfully applied to targeted delivery of oligonucleotide aptamers<sup>7</sup> and therapeutic antibodies<sup>35</sup>. Doxorubicin belongs to the class of anthracyclines that intercalate DNA and inhibit translation and transcription, and it is commonly used in cancer therapy. A previous study demonstrated that by engineering the global twist of dsDNA in DNA origami structures<sup>36</sup>, it is possible to tune the DNA intercalation process and capacity of Doxorubicin. In this thesis, we further applied this phenomenon to construct a DNA drug delivery vessel with controlled release properties.

## 2 MATERIALS AND METHODS

### 2.1 DESIGN AND FABRICATION OF DNA ORIGAMI NANOSTRUCTURES

#### 2.1.1 caDNAno

caDNAno<sup>37</sup> is a software developed to ease the process of 2D and 3D DNA origami nanostructure design (Figure 7). dsDNA helices are arranged in a honeycomb fashion and adjacent helices are cross-linked together via immobile holiday junctions to construct desired DNA origami nanostructures. After completing the design of our nanostructure, we can select the most optimal scaffold and export a list of oligonucleotides required for the assembly of the nanostructure.

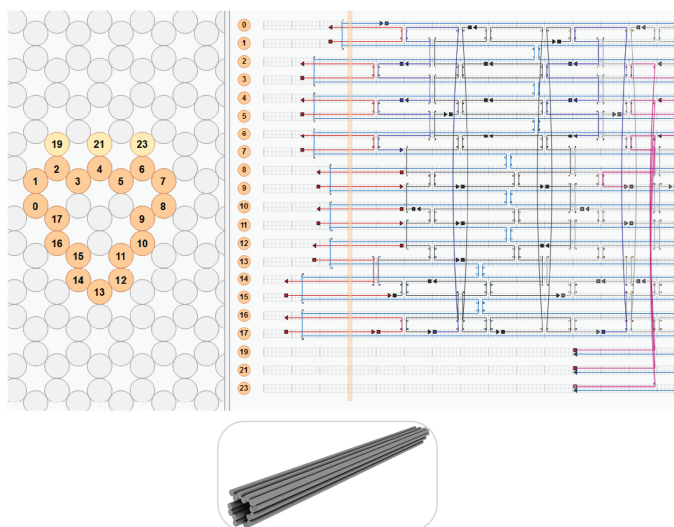


Figure 7. A snapshot of the caDNAno software and a maya 3D rendering of the 18HB.

In this thesis we used caDNAno to design an 18 helix bundle (18HB), a twisted 18 helix bundle, and a rectangular hollow brick and applied these DNA nanostructures to study cell signaling, antibody binding and drug delivery.

#### 2.1.2 Fabrication the DNA origami nanostructures

Engineered M13 phage genomic ssDNA was used as the scaffold (p7560 and p8634) for our DNA nanostructures, and they were prepared as described below:

A single colony of *Escherichia coli* JM109 was picked and transferred to 25 ml LB and cultured overnight at 37°C in a shaking incubator. 3 ml of the overnight culture was diluted into 250 ml 2xYT, and cultured in the same shaking incubator. The phages (p7560 or p8634) were added to the bacteria culture when its optical density reaches 0.5 at a multiplicity of infection (MOI) of 1, and the whole culture was incubated for an additional 5 hr. The culture was transferred into a 250 ml centrifuge bottle and centrifuged twice at 4000 rcf for 25 mins 4°C, transferring into a fresh centrifuge bottle in between. 10g PEG 8000 and 7.5g NaCl was added to the supernatant, and was incubated in an ice water bath for 30min. The supernatant



was then centrifuged at 10000 rcf for 30 mins 4°C, in this step the phages were pelleted. The phage pellet was then re-suspended in 10 ml Tris buffer (pH 8.5), added 10 ml of 0.2 M NaOH with 1% SDS, mixed gently by inversion and incubated for 3 min at room temperature. Afterwards, 7.5 ml of 3 M KOAc (pH 5.5) was added and the mixture was mixed gently by swirling, and incubated on ice for 10 min. The mixture was centrifuged at 16500 rcf for 30 min 4°C, and the supernatant, which contains the M13 ssDNA, was added 50 ml of 99.5% EtOH, mixed gently and incubated in an ice water bath for 30min before centrifuging at 16500 rcf for 30 min 4°C. The DNA pellet was washed with 75% EtOH, and centrifuged again at 16500 rcf for 10 min 4°C. The pellet was dried at room temperature for a minimum of 15 min, and re-suspended in 10 mM Tris (pH 8.5). The concentration of the ssDNA was measured with NanoDrop, and the quality and purity was characterized by agarose gel electrophoresis (1.5 % w/v agarose gel with 0.5 mg/ml ethidium bromide in 0.5x TBE as running buffer).

The staple oligonucleotides were ordered from bioneer, eurofins or integrated DNA technology. The staples were grouped into different subclasses (The core, protruding and anchoring staples) and pooled together to a final concentration of 400 nM for each oligonucleotide.

The nanostructures were folded in the following conditions: 20 nM M13 ssDNA scaffold, 100 nM for each staple (5 times excess to the scaffold), various MgCl<sub>2</sub> concentrations (13 mM for the 18helix bundle and 6 mM for the hollow brick), 5 mM Tris (pH 8.5) and 1 mM EDTA. The mixture was placed in a thermocycler, heated up to 80 °C for heat denaturation followed by a slow cooling process from 80 °C to 60 °C over 20 mins, and 60 °C to 24 °C for 14 hr. The folded structures were separated from excess oligonucleotides via Amicon ultrafiltration (described below). The quality of the folded and purified structures were accessed by running them on a 2% w/v agarose gel pre-stained with EtBr.

### **2.1.3 Bioconjugation between proteins and oligonucleotide handles**

Ephrin-A5-Fc and human IgG were purchased from R&D systems; horse spleen ferritin was purchased from Sigma-Aldrich. Amine modified oligonucleotides were ordered from either bioneer or integrated DNA technologies. Several different approaches were selected to perform the bioconjugation of our protein of interest to a handle oligonucleotide that allows further hybridization to the DNA nanostructures: Hydrazone click chemistry and two variants of copper free alkyne azide click chemistry that target either accessible lysine residues or His-tags.

Hydrazone click chemistry:

This method is separated into two sections: 1) 4FB (succinimidyl-4-formylbenzamide) modification of aniline modified oligonucleotides and 2) S-HyNic (succinimidyl-6-hydrazino-nicotinamide) modification of target protein and conjugation to the 4FB modified oligonucleotide.

1) 4FB modification of aniline modified oligonucleotides:

The 3 prime amine modified oligonucleotide was re-constituted to a concentration of 0.2 mM in , washed with the same buffer three times in a vivaspin 5k MWCO spin column (15000 rcf, 12 min room temperature) to remove unwanted residual chemicals, and concentrated to 2 mM. Sulfo-S-4FB was dissolved in anhydrous DMF (0.172M), and 12.5 uL was added to the concentrated oligonucleotide, and the mixture was incubated at room temperature for 1hr. An additional portion (12.5 ul) of Sulfo-S-4FB in DMF was added, and the mixture was incubated at room temperature for another hour. The modified oligonucleotides purified with ultrafiltration 8 times(Vivaspin 5k MWCO, 15000 rcf 12min room temperature, buffer: PBS pH 6.0), and concentrated to roughly 2 mM.

2) Sulfo-S-HyNic modification of target protein and conjugation to the 4FB modified oligonucleotide:

100 ug of lyophilized target protein was reconstituted in 100ul PBS pH 7.4 and washed with zeba spin desalting columns (7k MWCO) equilibrated with the same buffer. Sulfo-S-HyNic was dissolved in anhydrous DMF (7.3 uM). 2 ul Sulfo-S-HyNic was added to the protein solution, and incubated with occasional pipetting for 2 hr. The modified protein was buffer exchanged into PBS pH 6.0 with zeba spin desalting columns, and 10 ul of the 4FB modified oligonucleotide was added. The mixture was incubated at room temperature for 2 hr with occasional pipetting. Finally the oligonucleotide conjugated protein was purified with ultrafiltration (Amicon ultra 0.5, 50k MWCO, 10000 rcf 1 to 3 min per spin and a total of 8 spins). The protein concentration was quantified with the bradford assay, and conjugation efficiency (the concentration of the hydrazone bond) was quantified with UV-VIS, in particular the absorbance at 350 nm.

Copper free alkyne azide click chemistry:

1) Targeting lysine residues on the protein:

100 ug of target protein was reconstituted in 200 ul PBS (pH 7.4) and buffer exchanged to 100 mM NaCO<sub>3</sub> buffer (pH8.3) with zeba spin desalting columns (5k MWCO). Dibenzocyclooctyne-N-hydroxysuccinimidyl ester was dissolved in anhydrous DMF (5 mM), and was added to the target protein solution with 6 times molar excess, and the mixture was incubated at room temperature with occasional mixing for 4 hr. The protein mixture was buffer exchanged to PBS (pH7.4). The azide modified oligonucleotide was dissolved in PBS

(pH7.4) at a concentration of 100  $\mu$ M. The azide modified oligonucleotide was added to the protein mixture in a 10 times molar excess and the whole mixture was incubated at room temperature for 4 hr with occasional mixing. After the incubation, the protein-oligonucleotide conjugate was purified with ultrafiltration (Amicon Ultra 0.5, 50k MWCO, 10000 rcf, 1-3 min for each spin and a total of 8 spins). The final concentration of the conjugated protein was measured with the Bradford assay.

## 2) Targeting His-tags on the protein:

This protocol is carried out as in 1), but the protein was buffer exchanged to PBS (pH 6.3) and added 6 times molar excess of Bis-sulfone-PEG4-DBCO (10 mM in anhydrous DMF) to modify the protein. Conjugation to the azide modified oligonucleotide was carried out the same way as in 1).

### 2.1.4 Functionalization of DNA origami nanostructures

We have two approaches to functionalize our DNA origami nanostructures: 1) when working with heat sensitive substances such as proteins, we would conjugate the protein with an oligonucleotide handle and hybridize it to folded nanostructures and 2) when working with substances that can survive the heat denaturation process during the folding, we would include the functionalized oligonucleotides directly in the mixture of staples. In more detail:

1) We designed the nanostructures to express “pairs” of protruding oligonucleotides, with the protruding sequence complement to the handles on conjugated proteins, each pair of protruding oligo is defined as one protruding “site”. We can increase the hybridization yield dramatically by using pairs of protruding oligos instead of using single protruding oligos, and at the same time we observed that only one single protein-oligo conjugate can hybridize to the pair of protruding oligos. The nanostructures are adjusted to a final concentration of 20 nM and the conjugates were added in 5 times molar excess to each protruding site and incubated at 37°C for one hour, followed by a rapid cooling to 22°C and incubated at the same temperature for 14 hr.

2) Oligonucleotides that are modified with haptens (small molecule antigens) were incorporated directly in the DNA origami folding.

### 2.1.5 Purification of the functionalized DNA origami nanostructures

It is of crucial importance to fabricate our functionalized DNA origami nanostructures with high yield and purity, as contamination from productions materials (excess proteins) will introduce errors into our cell experiments or kinetics measurements. Below are the detailed protocols for the most reliable methods we used in this thesis:

## 1) Ultrafiltration with Amicon spin columns:

A maximum of 200  $\mu$ l 20 nM folded nanostructures was transferred into an amicon ultra 0.5 spin column, and spun at 10000 rcf for 1-2 mins at room temperature. A total of five to six spins was required to remove all excess staples.

Alternatively, when purifying protein modified nanostructures, we need to passivate the membrane to reduce non-specific binding and increase the recovery yield. The passivation was carried out by pipetting 400  $\mu$ l of 5% w/v pluronics into the columns and incubated overnight. The passivated column was washed with water six times before introducing the sample. Purification of the samples were carried out as described above (2.1.3).

## 2) Gel filtration with Sepharose 6B:

11 ml of crude Sepharose 6B size exclusion resins in 20% ethanol were bufferexchanged to PBS (pH 7.4) by repetitive centrifugation (800rcf, 1 min) and resuspension (in 50 ml PBS) for a total of six times. The final concentration of the resin slurry was adjusted to 50% v/v. The resins were loaded into empty spin columns, one column with 800  $\mu$ l slurry and another with 460  $\mu$ l slurry. The columns were placed on collection tubes with 1  $\mu$ l 1M  $MgCl_2$  loaded at the bottom, this is to replenish the  $MgCl_2$  that will be removed during the purification process, since we discovered that if the resins were equilibrated in PBS containing  $MgCl_2$ , the recovery yield decreases dramatically. The loaded columns were spun at 800 rcf for 1 min to remove the buffer. 100  $\mu$ l of nanostructures was passed through the two columns sequentially, first through the column loaded with 800  $\mu$ l slurry and second through the one loaded with 400  $\mu$ l slurry.

## 2.2 STUDYING BINDING KINETICS WITH SURFACE PLASMON RESONANCE

### 2.2.1 Ephrin-A5-Fc and EphA2 binding kinetics

Human EphA2 (extracellular domain) was immobilized on a CM3 chip. In detail: EphA2 was reconstituted at 1mg/ml, diluted 100 times into 10 mM Sodium Acetate buffer (pH 4.5) and injected over a NHS-EDC activated CM3 chip for 7 mins. EphrinA5-Fc and EphrinA5-Fc oligonucleotide conjugates were diluted to concentrations ranging from 12 to 120 nM in PBS (pH7.4) supplemented with 10 mM  $MgCl_2$ . Ephrin-A5-Fc nanocalipers were diluted to concentrations ranging from 6 to 24 nM. The samples were injected over the surface with a contact time of 15 min, and the binding curves were fitted with a 1:1 binding model to extract the binding affinity (KD). BIAcore 2000 was used to record the binding curves and BIAevaluation 3.2 software was used to process the data.

### 2.2.2 Antibody binding kinetics

Streptavidin was reconstituted to 1mg/ml, diluted 100 times in 10 mM Sodium Acetate Buffer (pH 4.5) and passed through an NHS/EDC activated CM3 chip with a contact time of

6 mins and 10 ul/min flowrate. Afterwards, 200 nM biotinylated anchor oligonucleotides were injected over the surface for 20 mins and a flowrate of 10 ul/min followed by a washing step with 50 mM NaOH for 5 min. Antigen nanopinboards expressing the complement of the anchor oligo was injected over the surface for 20 min at a flowrate of 2 ul/min. The immobilization processes were carried out at 25°C.

For the antibody binding experiments, we used BIAcore t200. Antibodies of interest were diluted to a concentration close to the range to its  $K_D$ , and a total of five increasing concentrations were injected sequentially with the single cycle kinetics method for 5 min each and a flowrate of 30 ul/min, followed by a dissociation step for 15 min. The binding curves were fitted with the t200 evaluation software, the on-rate, off-rate,  $K_D$  and binding capacity were extracted. Depending on the binding affinity of antibody-antigen binding, the experiments were performed at either 25°C (for binding affinities in the nM range) or 37°C (for binding affinities in the pM range).

## **2.3 CELLULAR SIGNALING EXPERIMENTS**

### **2.3.1 Cell culture and Eph receptor stimulation**

MDA-MB-231 cells were cultured in DMEM (Dulbecco's modified eagle medium) supplemented with 10% FBS (Fetal bovine serum) and 1% penicillin & streptomycin. The cells were cultured on 16-well or micropatterned glass slides for the immunohistochemistry and PLA experiments. The cells were seeded at 60000 cells/ml and unbound cells were washed away after 1hr incubation.

The cells were serum starved for one hour prior to EphA2 stimulation. EphrinA5 modified nanostructures were added to the cell culture medium to a final concentration of 10 nM Ephrin-A5-Fc concentration, and ephrinA5-Fc and clustered ephrinA5-Fc controls were added to the culture medium to reach the same ephrinA5-Fc concentration as the nanostructures. The stimulation lasted for 15 mins before fixing the cells with 10% formalin for 20 min.

The proximity ligation assay (PLA) was carried out as follows:

A PLA kit from Duolink was used in the section. The fixed cells were incubated with DUOLink II blocking solution in a humidity chamber (37°C). One anti-phosphotyrosine (1 to 1200x dilution) and one anti-EphA2 antibody (1 to 1500x dilution) was diluted in Duolink II antibody diluent buffer, introduced to the fixed cells and incubate overnight at 37°C. After the incubation, the samples were washed with Duolink II wash buffer for three times and 10 min each. The PLA probes (Duolink II anti-Mouse + and Duolink II anti-Rabbit -) were introduced to the samples and incubated for 60 min at 37°C, and washed three times for 10

min with Duolink II wash buffer. Afterwards the DNA ligase (1:50 dilution in ligase buffer) was added to the samples and incubated for 30 min at 37°C, and washed twice in Duolink II wash buffer for 2 min each wash. The samples were incubated 37°C for 60 min after the addition of the DNA polymerase diluted (1 to 160x dilution) in Duolink II amplification buffer. Finally the samples were washed two times with the wash buffer. The cells were stained with phalloidin and DAPI, and mounted with Vectashield. The cells were imaged with Zeiss Cell Observer fluorescent microscope.

### **2.3.2 Cell invasion assay**

The cell invasion assay was performed with ECM precoated cell culture inserts (8  $\mu$ m pores). The ECM layer was rehydrated by incubation in serum free medium for 2 hr at room temperature. The cells were collected with cell scrapers, followed by treatment with IgG, ephrin-A5 monomer, ephrin-A5-Fc, IgG clustered ephrin-A5-Fc, and the nanocalipers, at a final ephrin-A5 concentration of 20 nM for 15 min at 37°C. 40000 cells were seeded into each well and cultured for 24 hr and fixed with 10% formalin and permeabilized with 100% methanol. Non-invading cells were removed from the interior of the insert, the remaining cells were stained with antibodies from the supplier (Millipore) and DAPI. The cells were imaged with Zeiss Axioscope 2 microscope.

### 3 RESULTS AND DISCUSSION

We used the DNA origami method to create well-defined patterns of various biomolecules, and applied these patterned biomolecules to study cell signaling events and antibody binding. We also customized a selection of purification methods to achieve quality fabrication of these biomolecule-decorated DNA origami nanostructures. Finally we fabricated a DNA origami nanostructure with an engineered twist to deliver anticancer drugs in a controlled release fashion.

#### 3.1.1 Folding and functionalization of DNA origami nanostructures (Paper I)

We designed a selection of DNA origami nanostructures, one rod, one twisted rod and one rectangular brick with caDNAno. The rod was used to pattern antigens and ephrins; the twisted rod was used for drug delivery studies and the rectangular hollow brick was used to pattern antigens in 2D.

The folding of DNA origami structures generally requires the presence of divalent cations, such as Magnesium ( $Mg^{2+}$ ), to neutralize the negative charge repulsion between the phosphodiester backbones. But excess  $Mg^{2+}$  ions can crosslink the scaffolds and form aggregates of DNA. Different structures exhibit different amounts of crossovers and DNA packing density, therefore each DNA origami structure has a  $Mg^{2+}$  concentration “sweet spot” where its concentration is enough to neutralize the charge repulsion between DNA back bones and not high enough to aggregate the scaffold. For each DNA origami nanostructure we performed a magnesium concentration screening to find the optimal concentration for its folding (Figure 8).

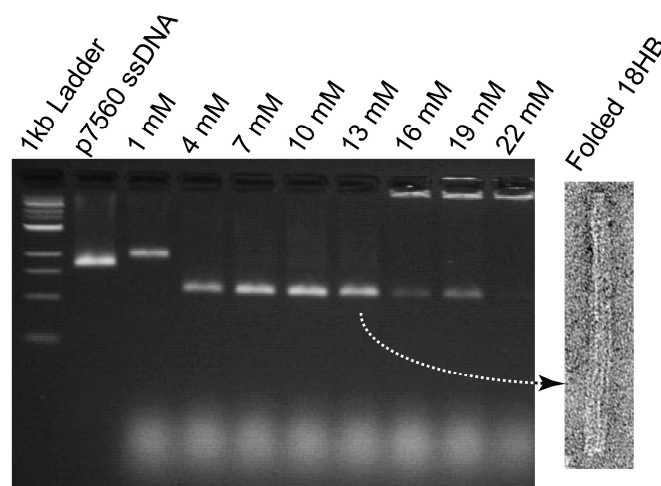


Figure 8. A standard magnesium screening experiment for DNA origami nanostructures. The 18HB was folded in a range of  $\text{MgCl}_2$  concentrations. At low  $\text{MgCl}_2$  concentrations (1 mM) the structures do not fold, resulting in a band that runs slower than the scaffold (p7560 ssDNA). As the  $\text{MgCl}_2$  concentration increases, the 18HB starts to fold, and between 10 and 13 mM reaches its optimal folding (fast running, intense and sharp bands). At high  $\text{MgCl}_2$  concentrations the folding start to aggregate ( $>16$  mM  $\text{MgCl}_2$ ). A transmission electron micrograph of a well folded 18HB at 13 mM  $\text{MgCl}_2$  is shown in the right panel, the box is 150 nm x 35 nm.

Functionalization of our DNA origami nanostructures were performed in two ways, depending on the functional group (Figure 2): 1) small chemicals that are thermo stable was conjugated directly to staple oligonucleotides and incorporated in the folding process. 2) Proteins or chemicals that are sensitive to heat are conjugated to a handle oligonucleotide and further hybridized to folded DNA nanostructures.

To quantify the functionalization yield of proteins, in particular ephrin-A5-Fc, a gel retardation assay was applied and successful hybridization of the ephrin-A5-Fc-oligonucleotide conjugates to the nanocalipers can be seen as retardation in the gel band (Figure 8a), and the retardation distance corresponds to the amount of proteins immobilized on the structures. We also used transmission electron microscopy (TEM) to image the ephrin-A5-Fc nanocalipers, and observed that the ephrin-A5-Fc appear as white clouds at the designed positions: 0 nm (NC0, a single ephrin-A5-Fc on the tip of the nanocaliper), 42.9 nm (NC40) and 101.2 nm (NC100) (Figure b-e).



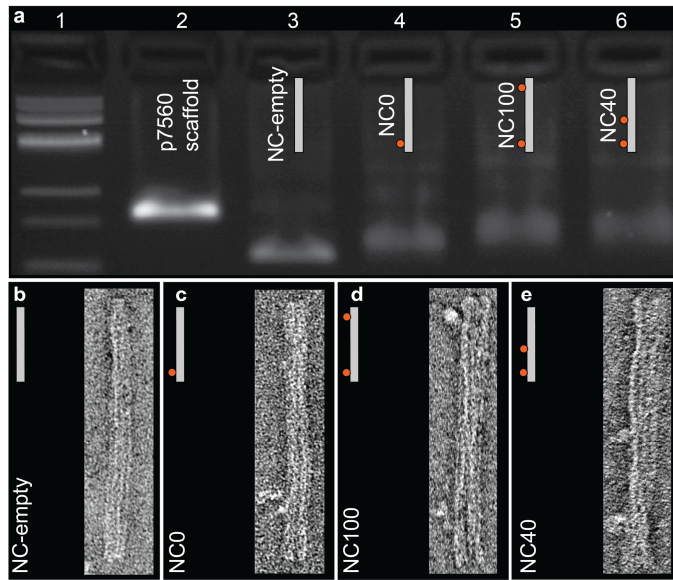


Figure 8. Characterization of ephrin-A5-Fc nanocalipers (NC empty, NC0, NC100 and NC40)<sup>6</sup>. a. Gel retardation assay (2% agarose gel pre-stained with EtBr) showing the gradual decrease in the migration speed of the nanocalipers as the number of immobilized ephrin increases. b-e. TEM micrographs (150 nm x 35nm) of the nanocalipers; the ephrins can be seen as white clouds at the designed distances (0, 42.9 and 101.2 nm).

### 3.1.2 Characterization of the bio-availability of ephrin-A5-Fc nanocalipers (Paper I)

It is crucial to characterize the bio-availability of the proteins immobilized on the DNA origami nanostructures. In the case where we produced ephrin-A5-Fc nanocalipers, we used surface plasmon resonance (SPR) to compare the binding constants of unconjugated ephrin-A5-Fc, oligonucleotide conjugated ephrin-A5-Fc and ephrin-A5-Fc nanocalipers (Figure 9). We immobilized the EphA2 receptor on the SPR surface and flown over the ephrins and nanocalipers at various concentrations, which would give us a series of binding curves. After fitting the binding curves with a 1:1 Langmuir binding model, we obtained the binding constants, and the results are shown in figure 9.

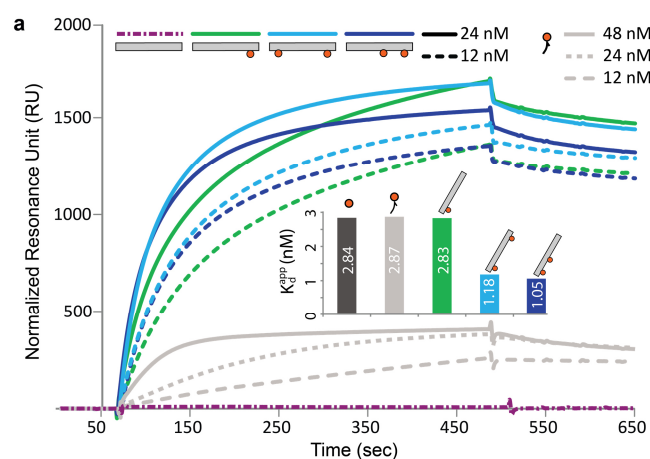


Figure 9. Surface plasmon resonance characterization of ephrin-A5-Fc conjugates and ephrin-A5-Fc nanocalipers<sup>6</sup>. Binding curves of ephrin-A5-Fc conjugates (grey curves) and ephrin-A5-Fc nanocalipers (green, blue and purple curves) to immobilized extracellular domain of human EphA2. The curves were fitted with a 1:1 Langmuir binding model and the apparent dissociation constants were obtained, and shown in the inset.

The results show that the unmodified ephrin, conjugated ephrin and nanocalipers modified with one ephrin-A5-Fc (NC0) exhibits similar binding affinity towards EphA2, indicating that the bio-availability of these proteins were retained throughout the production process. Moreover, we saw an increase in the binding affinity for the two nanocalipers decorated with two ephrins-A5-Fc, indicating that there is an avidity effect and the bio-availability of both ephrin-A5-Fc were retained (Figure 9).

To further investigate whether the ephrin-A5-Fc nanocalipers can bind to EphA2 expressing cells, we performed fluorescence activated cell sorting (FACS) experiments (Figure 10). We observed that cells that were treated with IgG-clustered ephrin-A5-Fc and ephrin-A5-Fc nanocalipers showed similar FACS signals, indicating that the cells were bound with ephrin-A5-Fc ligands.

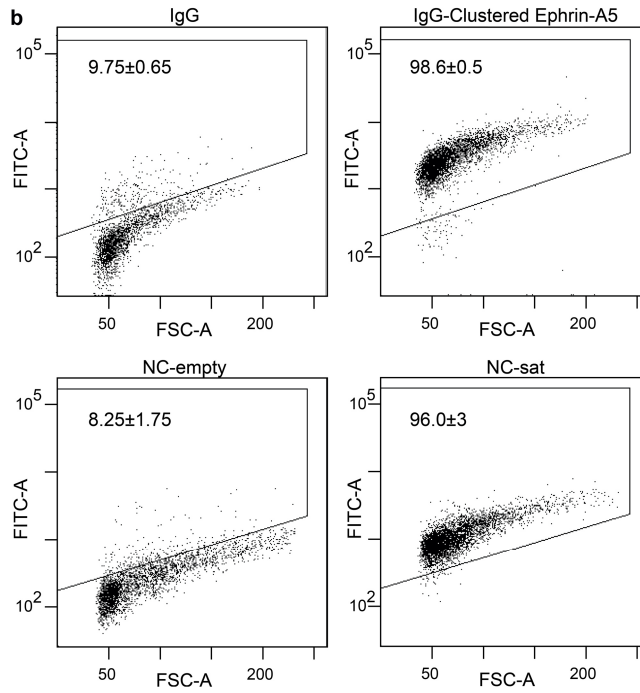


Figure 10. FACS analysis of IgG clustered ephrin-A5-Fc and ephrin-A5-Fc nanocalipers binding to MDA-MB-231 cells<sup>6</sup>. Alexa-488 conjugated anti-human IgG was used to target the Fc region on the ephrin-A5-Fc.

### 3.1.3 Spatial regulation of EphA2 receptor activation (Paper I)

We applied the proximity ligation assay<sup>38</sup> (PLA) to quantify the EphA2 activation level, and we cultured the MDA-MB-231 cells on fibronectin micropatterns to prevent cell-cell contact-induced EphA2 activation.

First we studied the activation of EphA2 with conventional IgG-clustered ephrin-A5-Fc, ephrinA5 monomer and dimers (ephrin-A5-Fc), and only IgG-clustered ephrin-A5-Fc was described to activate EphA2 efficiently. We observed a gradual increase in the EphA2 activation level in the cells stimulated with the monomer, dimer and cluster, which is in line with previous studies, and indicating that the PLA assay is valid (Figure 11a and b).

Next we studied EphA2 activation with ephrin-A5-Fc nanocalipers. We engineered the nanostructures to present either one ephrin-A5-Fc (NC0) or two ephrin-A5-Fc at 42.9 nm (NC40) and 100.3 nm (NC100). Cells stimulated with NC0 and NC100 showed similar EphA2 activation level, indicating that the two ephrin-A5-Fc failed to pose a collaborative effect on its activation. Cells treated with NC40 however, showed an increase in the EphA2 activation level compared to that of NC0 and NC100, indicating that two ephrin-A5-Fc placed at 40 nm can elicit a proximity effect in the activation of the receptor (Figure 11c and d).

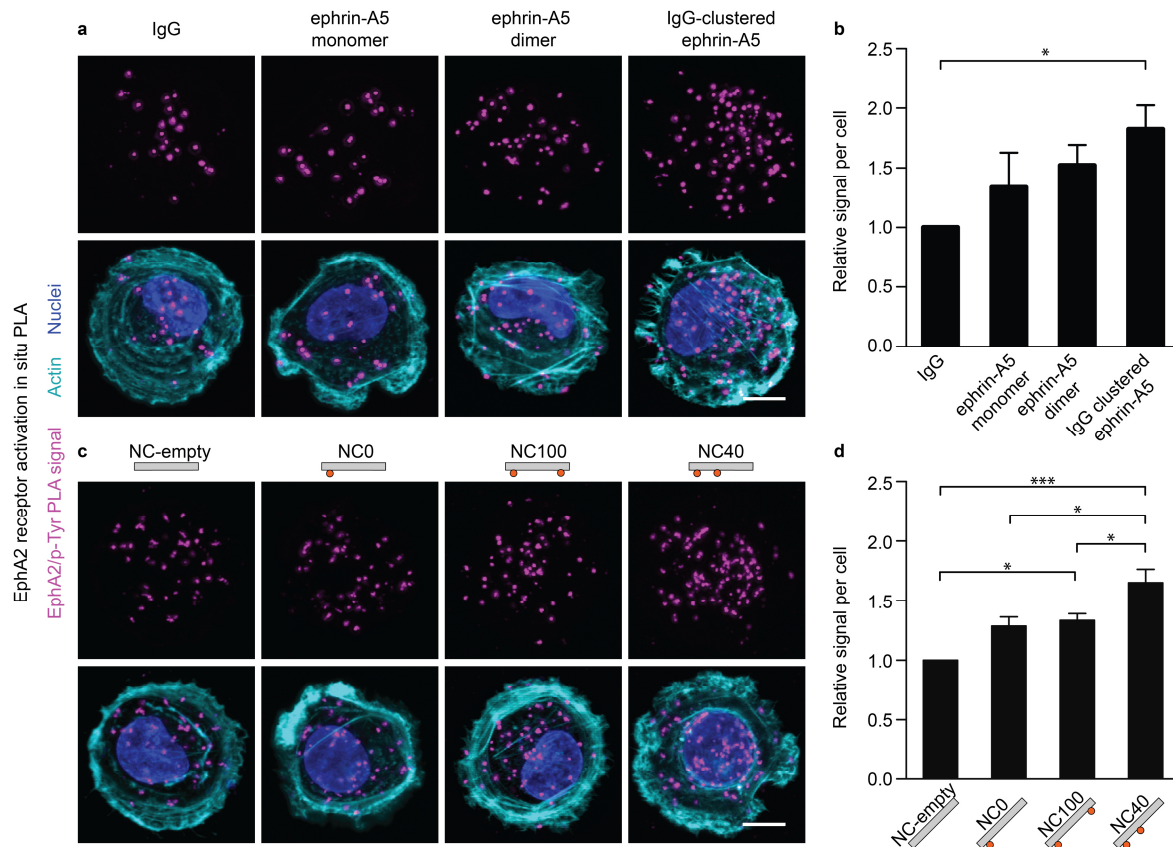


Figure 11. Proximity ligation assay to quantify EphA2 activation in MDA-MB-231 cell line<sup>6</sup>. a and c. each magenta dot represents activated EphA2; actin is presented in cyan and the nuclei in blue. scale bar: 10  $\mu$ m. b and d. quantification of magenta dots per cell and normalized to cells treated with either IgG or NC empty control. A minimum of N=5 was performed for each data point. Error bars are s.e.m.

Activation of the EphA2 receptor in cancer cells with recombinant ligands was shown to decrease cell invasion properties<sup>39</sup>. We further characterized downstream events of the EphA2 receptor activation and study the change in the treated cell line's invasive properties. We observed a similar trend as the EphA2 activation in the decrease in cell invasion of the ephrin-A5-Fc nanocaliper treated cells: NC40, which is more potent in activating EphA2 resulted in a stronger decrease in cell invasion, while NC100 that is less potent in activating EphA2 resulted in a weaker decrease in cell invasion (Figure 12).

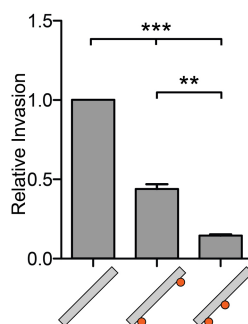


Figure 12. Ephrin-A5 nanocalipers direct the invasive properties of MDA-MB-231 cells<sup>6</sup>. The relative fold decrease in matrix invasion of cells treated with NC empty, NC100 and NC40 was quantified. \* P value < 0.05, \*\* P value < 0.01, \*\*\* P value < 0.001.

### 3.1.4 Studying antibody flexibility and complex antigen binding with PSPR (Paper II)

We explored the flexibility of various antibodies by arranging two small molecule antigens at distances ranging from 2 nm to 28 nm with the patterned surface plasmon resonance (PSPR) method. We monitored the ability of the antibodies to cross-link the two antigens (Figure 13 top panel), which would result in a bivalent binding and a significantly increased apparent binding affinity. We first studied the flexibility of commercially available anti-digoxigenin antibodies due to its high affinity and specificity, and we observed a U-shaped behavior when its binding affinity was plotted against antigen distances. Bivalent bindings between two antigens and an antibody were observed to exhibit weakened binding affinities when the two antigens were placed at close (2-3 nm) or far (15-17 nm) distances. We hypothesize that physical stress is posed on the antibody's hinge region when the two Fab arms try to come close to bind to close distances, or try to stretch to bind to farther distances, both deviating from the two arm's natural distance distribution. As a result, this stress will translate to a strained antibody conformation and decreased binding affinity. We also studied the binding behavior of antibodies with lower binding affinities (Figure 13 bottom panel) and observed that these antibodies failed to crosslink at the short and long distances, indicating that the binding energy is insufficient to introduce stress in the hinge region to allow the two Fab arms to cross-link the close and far antigens.

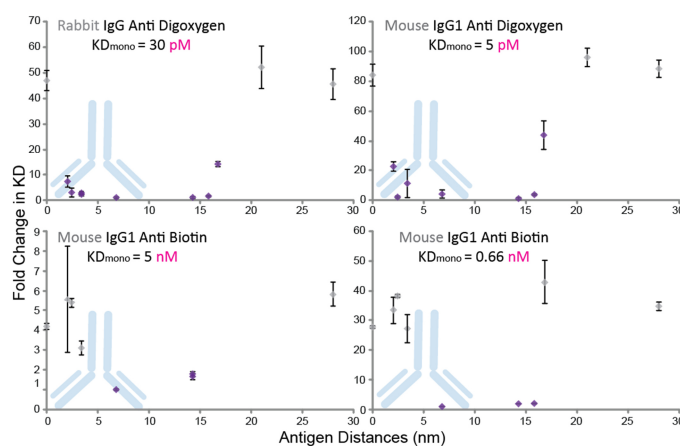


Figure 13. Applying PSPR to study the flexibility of various antibodies. x-axis: distance between two antigens on the same nanopinboard (0 nm distance is an antigen monomer); y-axis: fold change in the apparent dissociation constant ( $K_d$  app) with the strongest bivalent binding set to a value of 1. Grey dots represent monovalent binding, purple dots represent bivalent binding.

We applied the PSPR method to present antigens at various amounts and patterns, and study the complex interactions between multiple antibodies and antigens (Figure 14). First we performed a series of control experiments, to demonstrate the programmability and reliability of the PSPR method to arrange antigens: antigen monomers (JR1) is a monovalent binding control, antigen dimers are arranged either as close dimers (JR2c) to allow bivalent binding, or distant dimers (JR2f) to allow only monovalent binding, the antigen trimer (JR3f) control was arranged so that three antigens are placed further apart, also only allowing monovalent binding. Results show that we have satisfactory control of the antigen orientations: JR1, JR2f and JR3f showed monovalent binding with binding capacities of one, two and three antibodies respectively, and bivalent JR2 showed a strong bivalent binding with a binding capacity of one antibody (Figure 14).

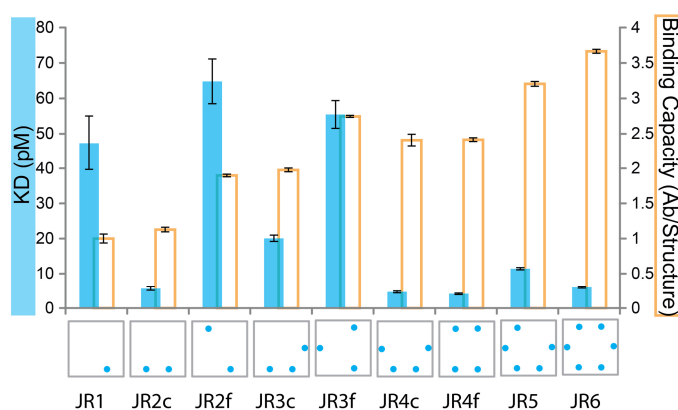


Figure 14. Applying the PSPR method to study multimeric antigen-antibody interactions. The measured apparent  $K_D$  is plotted as blue columns; the orange secondary axis represents the binding capacity of each structure normalized to the monovalent control (JR1). Illustrations of the antigen patterns are presented at the bottom of the plot (grey square: nanopinboard, blue dots: antigen (in this case digoxigenin)), error bars are standard deviation, c: closely arranged antigens, f: antigens arranged at farther distances.

To study how antibodies interact with more complex antigen patterns with biological relevance, we applied the PSPR method to express antigen trimers, tetramers, pentamers and hexamers (Figure 14). Antigen trimer (JR3c and JR3f) and tetramers (JR4c and JR4f) were arranged both as closely packed clusters or separate monomers or two separate dimers. The antigen pentamer (JR5) and hexamer (JR6) were placed on vertices of a hexagon. The binding affinity of the close antigen trimer (JR3c) was between that of monovalent and bivalent binding, with a binding capacity of two antibodies. This indicates that the binding consists of a 1:1 mixture of monovalent and bivalent binding, and can be supported by our binding kinetics simulation. Both the closely placed tetramer (JR4c) and the double separate dimer (JR4f) resulted in 2 bivalent bindings. The pentameric antigen (JR5) shows a binding affinity between the close trimer and a bivalent binding, and it has a binding capacity of three antibodies. This indicates that the binding consists of a 2:1 ratio of bivalent: monovalent binding. The antigen hexamer (JR6) is particularly interesting since antibody hexamers that self-assemble on foreign organelles were believed to play a key role in the activation of the complement system<sup>24</sup>. This requires the presence of at least six antigens in close proximity. However, our results show that the most dominant binding population in this scenario is three bivalent binding.

### **3.1.5 Purification of functionalized DNA origami nanostructures (Paper III)**

To determine the purification efficiency of all seven methods tested in this study we used agarose gel electrophoresis (AGE) to examine the integrity and the recovery yield of the functionalized DNA origami structures. TEM imaging was used to complement AGE. The recovery yield was calculated by comparing the gel band intensity of purified functionalized 18HB to that of unpurified functionalized 18HB. Contamination was quantified by carrying out the same purification protocols with samples containing only conjugates, and the concentration of residual conjugates (the contaminants) were measured. Three repeats were performed for each data point.



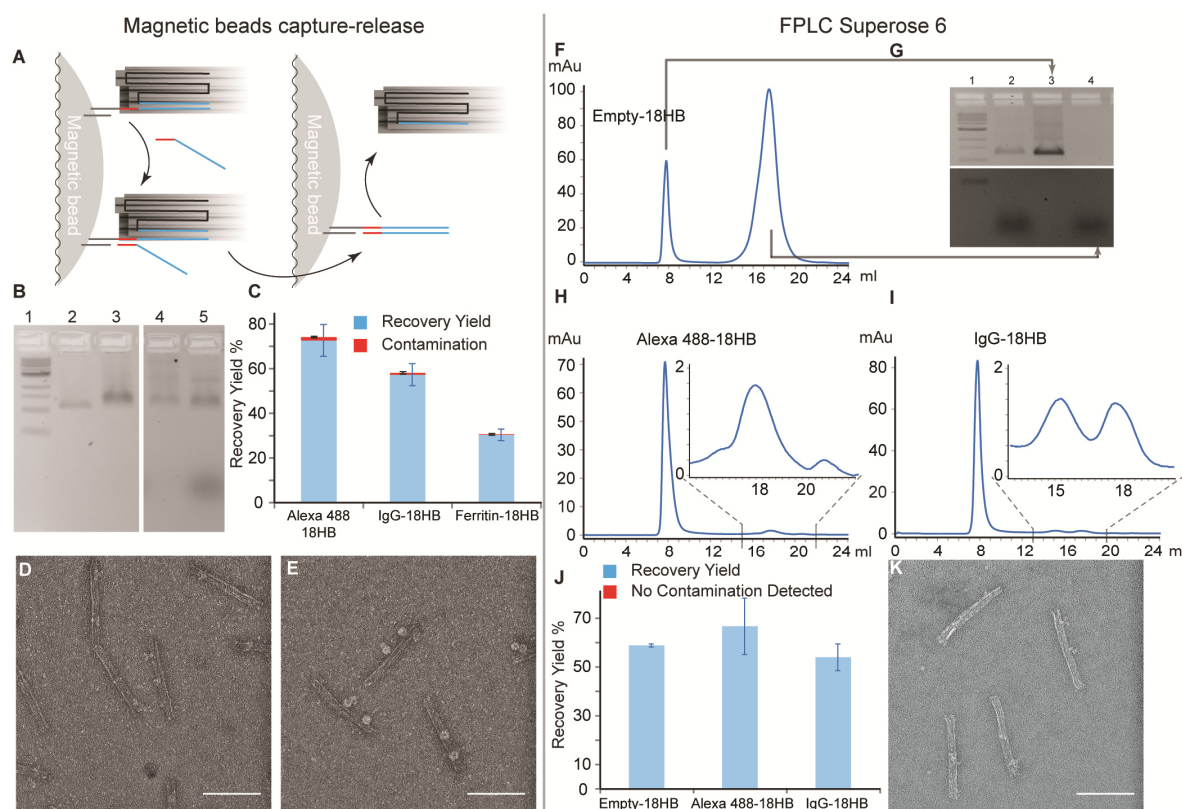


Figure 15. The two methods we adapted to purify functionalized DNA origami<sup>28</sup>. a. the magnetic beads capture-release procedure (structures were folded with an extra staple that can bind to the poly T magnetic beads. After washing, invader oligonucleotides (the red-blue line) was added, the invader would bind first partially to the linker oligonucleotide (red line) and subsequently replace the linker-bound nanostructure and releasing the nanostructure). b. 2% agarose gel pre-stained with EtBr. Lane 1, 1kb DNA ladder; lane 2, empty 18HB; lane 3, non-purified IgG-18HB; lane 4, the fraction of IgG-18HB that was not captured by the beads; lane 5, purified IgG-18HB released from the beads. c. summary of recovery yields from the magnetic bead purification method  $n=3$ . d and e, TEM micrographs of magnetic bead purified IgG-18HB (d) and ferritin-18HB (e). f. a chromatogram of the empty 18HB purified with FPLC (superpose 6 column), the 18HB elutes at 8 ml while staples from the folding elutes at 17 ml. g. 2% agarose gel pre-stained with EtBr showing the content of each peak from f, the staple band in the lower section of the gel was contrast enhanced for visualization purposes. h and i, chromatograms of A488-18HB and IgG-18HB purified with FPLC, the A488 and IgG conjugates elute at 18 ml and 15-18 ml respectively. j. summary of recovery yields from FPLC purification  $n=3$ . k. TEM micrograph of FPLC purified IgG-18HB. All TEM scale bars are 100 nm, error bars are standard deviations.

Samples purified with the magnetic bead capture method resulted in recovery yields around 70% for A488-18HB, 57% for IgG-18HB and 30% for ferritin-18HB (Figure 15a-e). We suspect the relatively low recovery yield for ferritin-18HB is due to unspecific interactions between the beads and ferritin. We observed that IgG interacts unspecifically with the beads as well, but this interaction can be reduced by the addition of a nonionic detergent: poloxamer, which is commonly used in cell culture systems to reduce the damage from stirring or liquid flow. The magnetic bead capture method offers a high purification efficacy, which is independent of the type of contaminants as all three types of conjugates all



resulted in high purity. From this, we suggest that this method is a potential universal method for the purification of functionalized DNA origami nanostructures.

We observe the recovery yield of FPLC experiments were sensitive to the concentration of divalent cations such as  $Mg^{2+}$ , which could be the result of two effects combined: 1)  $Mg^{2+}$  can bridge the negatively charged DNA phosphodiester backbone with the lone pairs of the hydroxyl groups on the agarose-based Superose resin. 2) DNA origami nanostructures are densely packed double stranded DNA, which renders the local charge density relatively high compared to free M13 single stranded DNA. This hypothesis can be supported by our experimental results: the recovery yield of the M13 single stranded DNA is significantly higher than that of folded 18HB. To resolve this issue we tested a selection of buffers with various salt concentrations, and discovered that the optimal  $Mg^{2+}$  concentration is 3 mM in PBS (lower  $Mg^{2+}$  concentration will denature the 18HB).

The 18HB and all three types of conjugates were injected separately. The 18HB elutes at 8 ml, staples oligonucleotides from the folding elute at 17 ml, IgG conjugates elute at 15 ml and 18 ml, A488 conjugates elute at 18 ml. These results indicate full separation of the conjugates from the 18HB. The recovery yield is around 50% to 60% and comparable to the common methods (Figure 16), while offering high sample purity (Figure 15f-k).

The five common, previously published purification methods were first further fine-tuned to achieve optimal purification efficacy for further equal comparison (Figure 16).

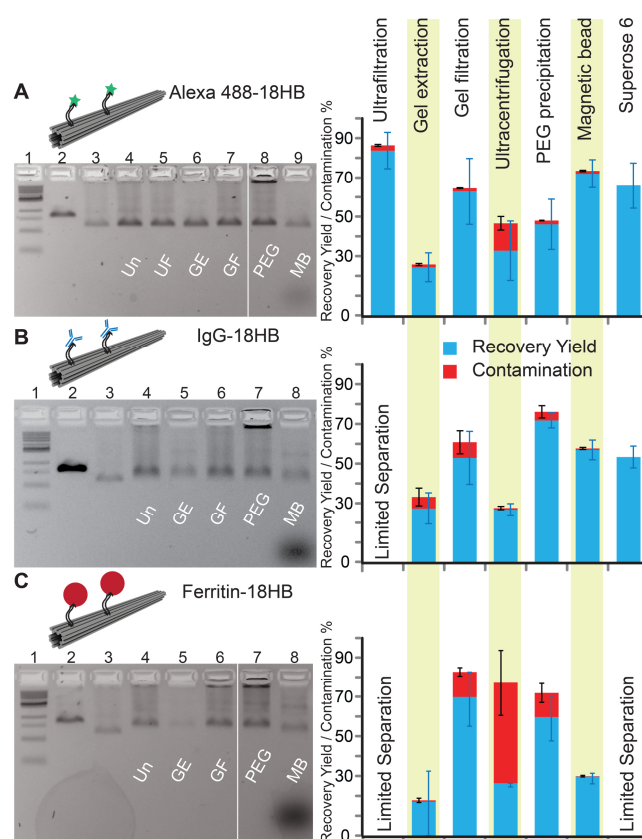


Figure 16. A summary of the recovery yield and contamination for all purification methods tested in this study<sup>28</sup>. All gels are 2% agarose gels pre-stained with EtBr. a. purification of A488-18HB. b. purification of IgG-18HB. c. purification of ferritin-18HB. Un: unpurified functionalized 18HB; UF: ultrafiltration; GE: gel extraction; GF: gel filtration; PEG: fractionation; MB: magnetic bead capture. Error bars are standard deviations.

Ultrafiltration filters can be passivated with proteins or chemicals to reduce non-specific interactions with the sample. Bovine serum albumin (BSA) and tween are common passivation reagents, but they either clog the membrane (BSA) or are cytotoxic (Tween). We discovered that the cell culture friendly detergent poloxamer is a potent passivation reagent. Ultrafiltration filters passivated with poloxamer (described above), exhibit higher recovery yield and at the same time maintain the filter's purification efficiency.

Agarose gel extraction is one of the most widely used methods to purify DNA origami nanostructures, but its extensive hands-on time and poor recovery yield has limited its application to mainly TEM sample preparation.

Gel filtration resins with the optimal cutoff can trap small molecules such as proteins and oligonucleotides while macromolecules like DNA origami nanostructures are eluted in the void volume. We discovered that divalent cations such as  $Mg^{2+}$  reduce the recovery yield of this method, possibly via the same mechanisms as the FPLC experiments. To resolve this issue we first equilibrate the resins in PBS without  $Mg^{2+}$ , and introduce a 1ul droplet of 1M  $MgCl_2$  to the collection tube, so that the eluted DNA origami is immediately replenished with  $Mg^{2+}$  and maintain the structure's integrity<sup>28</sup>.

PEG precipitation can result in aggregation of the purified samples, which is possibly due to the extensive concentration process.

The three methods that gave the best recovery yield for Alexa488-18HB are ultrafiltration, magnetic bead capture and gel filtration, with 84%, 72% and 63% recovery yield respectively. These methods were fairly potent in the removal of excess conjugates (near 98% removal) (Figure 16).

The three methods that gave the best recovery yield for IgG-18HB are: PEG fractionation, magnetic bead capture and gel filtration, with 72%, 57% and 53% recovery yield respectively. Both the magnetic bead capture and ultracentrifugation method were able to remove around 98% of excess IgG conjugates (Figure 16).

The two methods that gave the best recovery for ferritin-18HB are gel filtration and PEG precipitation, with recovery yields around 70% and 60% respectively. All purification methods generally resulted in reduced efficiency in the removal of ferritin, possibly due to its larger hydrodynamic radius. However, the magnetic bead capture method removed more than 99% of the ferritin conjugates (Figure 16).

### **3.1.6 DNA origami drug delivery system with tunable release properties (Paper IV)**

We designed two 18-helix bundle nanotubes to investigate the potency of DNA nanostructures as drug delivery vessels. First, we designed an 18-helix bundle structure (S-NANO) with a conventional 10.5 bases per helical turn (Figure 17a). Second we modified the 18-helix bundle to an unnatural 12 bases per turn (T-Nano, Figure 17b), which would induce a stress in the structure and the structure will adapt to a global right hand twist. Intercalation of DOX into dsDNA would change its pitch from 10.5 to 12 bases per turn. In accordance to this effect, S-NANO folded in the presence of DOX resulted in deformed structures (Figure 17c, slow-running bands in lane 3-5) while T-NANO was folded into straight, non-twisted structures in the presence of DOX (Figure 17d and f).

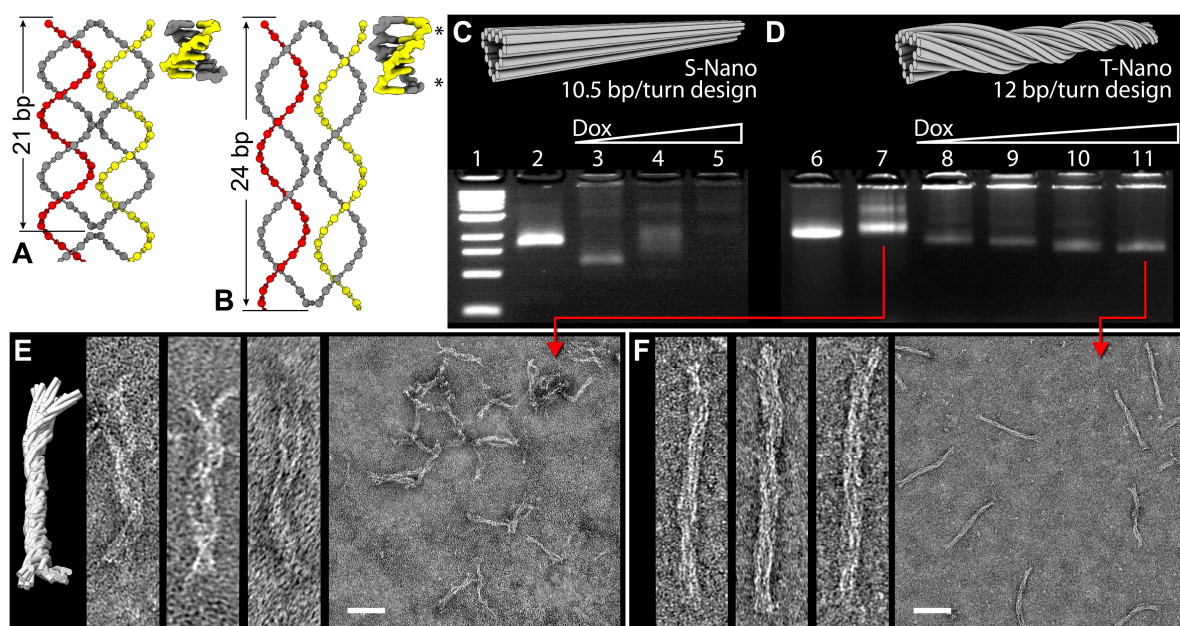


Figure 17. S-NANO and T-NANO<sup>9</sup>. a and b. DOX intercalation changes the twist of DNA from 21 base pairs per full turn to 24 base pairs per full turn. c. the folding quality of S-NANO deteriorates along with the increasing concentration of DOX. lane 1: 1kd DNA ladder, lane 2: p7560 ssDNA, lane 3-5: folding of S-NANO in the presence of DOX (16-96  $\mu$ M). d. the folding quality of T-NANO increases along with the addition of DOX. Lane 6: p8634 ssDNA, lane 7-11: folding of T-NANO in the presence of DOX (16-96  $\mu$ M) e. canDo simulation of T-NANO without the presence of DOX. e and f. TEM micrographs of T-NANO without (e and with DOX (f), the scale bars are 100 nm.

*In vitro* drug release properties of S-NANO and T-NANO loaded with DOX were measured and compared. In addition, the M13 dsDNA was also included as an extra control. We observed significant differences between the drug release kinetics of S-NANO, T-NANO and M13 dsDNA, the T-NANO was able to retain DOX for longer periods of time compared to S-NANO, for example, 50% of DOX was still retained by the structures after several hours of incubation. Interestingly, we observe no significant difference in the drug release kinetics between S-NANO and dsM13 DNA (Figure 18a).

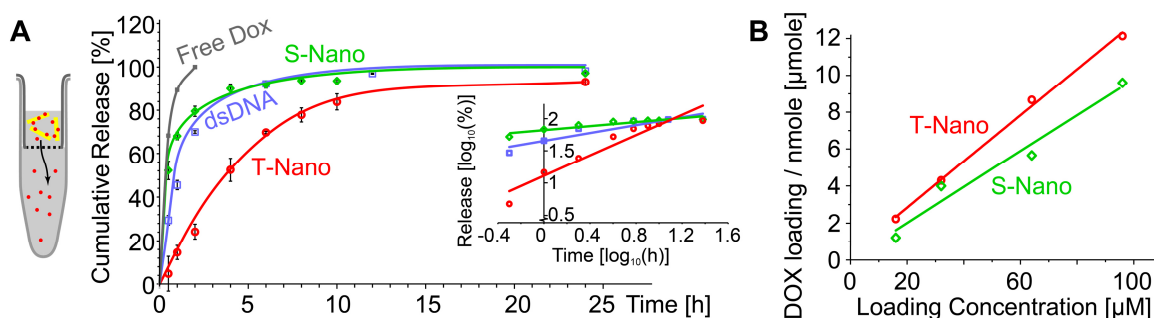


Figure 18. Drug release kinetics of our DNA nanostructures<sup>9</sup>. a. DOX, either in its free form or loaded in DNA was placed in a dialysis filter, and the diffusion of DOX across the membrane was measured via the fluorescence of DOX. The plot shows the concentration of diffused DOX plotted against time. b. the DOX loading capacity of S-NANO and T-NANO. x-axis: the concentration of DOX used to equilibrate the structures with; y-axis: the concentration of DOX bound to the DNA nanostructures measured via fluorescence, immediately after buffer exchanging and removal of excess DOX with ultrafiltration.

Prior to applying T-NANO to *in vitro* drug delivery experiments, we characterized its stability in cell culture medium via a gel shift assay, and observed that T-NANO is stable in cell culture medium within the time span of *in vitro* experiments (Figure 19a).

Current opinion suggests that DNA structures are degraded in the endosomes after being endocytosed<sup>40</sup>. We studied the capacity of DOX loaded T-NANO to kill cancer cells with a sulforhodamine B colorimetric assay. Three breast cancer cell lines were chosen as model systems: MDA-MB-231, MDA-MB-468 and MCF-7. The half-maximal inhibitory concentration (IC<sub>50</sub>) of DOX while delivered via T-NANO is significantly lower compared to that of DOX when added as its free form and DOX loaded in S-NANO (Figure 19b).

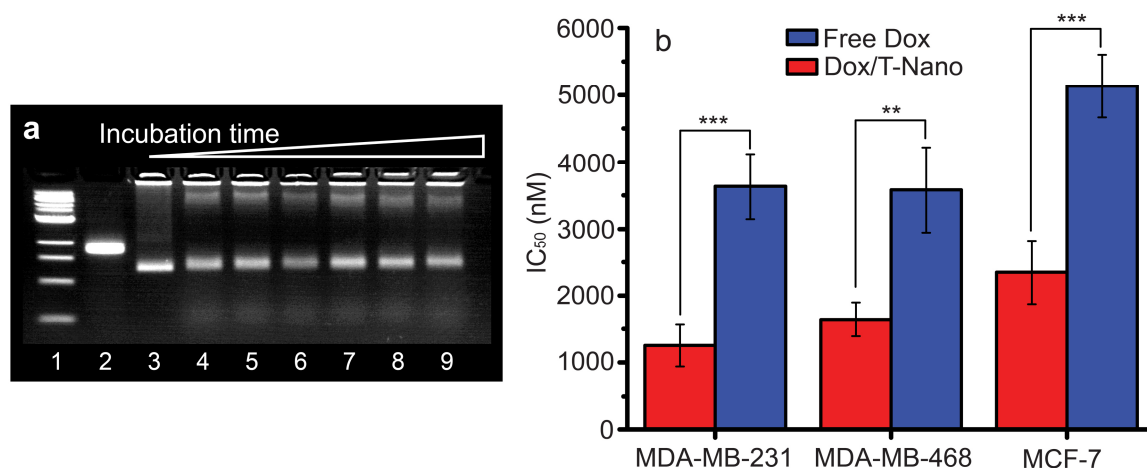


Figure 19. Stability and Toxicity of T-NANO<sup>9</sup>. a. 2% Agarose gel electrophoresis pre-stained with EtBr (Lane 1: 1kb DNA ladder, lane 2: p8634 ssDNA, lane 3: non-incubated T-NANO), showing the results of the incubation of T-NANO in the absence of DOX in cell culture medium (supplemented with 10% FBS) for 30min, 1 hr, 3 hr, 6 hr, 12 hr, 24 hr and 48 hr (lane 4-9). b. Cytotoxicity of free DOX (blue columns) compared that of DOX loaded T-NANO (red columns). N=4, \*\* p value <0.01, \*\*\* p value <0.001, error bars: standard deviation.

Our results indicate that by applying a global twist to DNA origami nanostructures, it is possible to increase its DOX loading capacity and decrease its drug release kinetics, rendering these twisted nanostructures a potent candidate for drug delivery vessels.

## 4 ACKNOWLEDGEMENTS

My co-workers know how much I love to use tables to document my experiments. As an icon of my gratitude and highest respect for all the amazing people I have work with and spent my life with, here is a table:

Name:	Thank you for:
Björn Högberg	Thank you for your scientific supervision and giving me the freedom to explore the exuberant world of DNA origami.
Ana Teixeira	Thank you for the great collaboration and your patience to answer all my cell biology related questions.
Andreas Nyström	Thank you for the inspirational chemistry discussions.
Agneta Ritcher-Dalfors	Thank you for establishing the great work environment in which I started my PhD journey.
Adolf Gogoll	Thank you for your amazing lectures in organic chemistry and for being my mentor.
Vanessa Lundin, Ekaterina Petrova	Thank you for the great collaboration with the nanocalipers project ☺.
Erik Benson	Haha you get your individual section as requested! ☺ Thank you so much for the great collaboration/traveling/scientific and non-scientific discussions.
Ioanna Smyrlaki	Haha you get your individual section too! ☺ Thank you for the great company when we were working weird hours.
Cosimo Ducani, Ferenc Fördös, João Rosa, Giulio Bernardinelli, Esther Fernandez Gonzalez, Ian Hoffecker	You guys are the best colleagues and friends, thank you for making my PhD studies vivid.
Corinna Kaul, Yong-Xing Zhao, Johan Gardell, Monika Schultz, Ian Woods, Camilla Sandén, Pavan Kumar Areddy	Thank you for the great company in the hogberg lab all these years. Wish you all the best for your career.
Friends: Alan#3 & Jenny, 皓鈞, 龜龜, 變態諺, 俊宏, 崇紋, 崇淵, 哈密瓜, 摩斯拉, 呆呆翔, 毛毛, Tughan Akbasak, Matias Funes	Thank you for the great friendship and support in the past one or two decades.
My Parents in-law	Thank you for all the help with babysitting Elvin, which allows me to work normal hours.
My Parents	Thank you for everything you have done, I owe everything I am today to you.
My little Brother Brian	Thank you for all your help and keeping mom and dad company all these years.
My lovely wife Xueshu	Thank you for coming into my life and made it as colorful as it can be. Let's continue the awesomeness of our small family.
My cute little boy Elvin	Thank you for choosing me as your dad, you have brought immense happiness into my life.

## 5 REFERENCES

- (1) Chen, J. H.; Seeman, N. C. Synthesis from DNA of a Molecule with the Connectivity of a Cube. *Nature* **1991**, *350*, 631–633.
- (2) Rothemund, P. W. K. Folding DNA to Create Nanoscale Shapes and Patterns. *Nature* **2006**, *440*, 297–302.
- (3) Tørring, T.; Helmig, S.; Ogilby, P. R.; Gothelf, K. V. Singlet Oxygen in DNA Nanotechnology. *Acc. Chem. Res.* **2014**, *47*, 1799–1806.
- (4) Bai, X.-C.; Martin, T. G.; Scheres, S. H. W.; Dietz, H. Cryo-EM Structure of a 3D DNA-Origami Object. *Proc. Natl. Acad. Sci. U. S. A.* **2012**, *109*, 20012–20017.
- (5) Douglas, S. M.; Bachelet, I. Transport of Molecular Payloads. *Science* **2012**, 831–834.
- (6) Shaw, A.; Lundin, V.; Petrova, E.; Fördös, F.; Benson, E.; Al-Amin, A.; Herland, A.; Blokzijl, A.; Högberg, B.; Teixeira, A. I. Spatial Control of Membrane Receptor Function Using Ligand Nanocalipers. *Nat. Methods* **2014**, *11*, 841–846.
- (7) Schüller, V. J.; Heidegger, S.; Sandholzer, N.; Nickels, P. C.; Suhartha, N. A.; Endres, S.; Bourquin, C.; Liedl, T. Cellular Immunostimulation by CpG-Sequence-Coated DNA Origami Structures. *ACS Nano* **2011**, *5*, 9696–9702.
- (8) Jiang, Q.; Song, C.; Nangreave, J.; Liu, X.; Lin, L.; Qiu, D.; Wang, Z. G.; Zou, G.; Liang, X.; Yan, H.; *et al.* DNA Origami as a Carrier for Circumvention of Drug Resistance. *J. Am. Chem. Soc.* **2012**, *134*, 13396–13403.
- (9) Zhao, Y.-X.; Shaw, A.; Zeng, X.; Benson, E.; Nyström, A. M.; Högberg, B. DNA Origami Delivery System for Cancer Therapy with Tunable Release Properties. *ACS Nano* **2012**, *6*, 8684–8691.
- (10) Kuzyk, A.; Schreiber, R.; Fan, Z.; Pardatscher, G.; Roller, E.-M.; Högele, A.; Simmel, F. C.; Govorov, A. O.; Liedl, T. DNA-Based Self-Assembly of Chiral Plasmonic Nanostructures with Tailored Optical Response. *Nature* **2012**, *483*, 311–314.
- (11) Kolb, H. C.; Finn, M. G.; Sharpless, K. B. Click Chemistry: Diverse Chemical Function from a Few Good Reactions. *Angew. Chemie - Int. Ed.* **2001**, *40*, 2004–2021.
- (12) Kalia, J.; Raines, R. T. Advances in Bioconjugation. *Curr. Org. Chem.* **2010**, *14*, 138–147.
- (13) Jewett, J. C.; Bertozzi, C. R. Cu-Free Click Cycloaddition Reactions in Chemical Biology. *Chem. Soc. Rev.* **2010**, *39*, 1272–1279.
- (14) Cong, Y.; Pawlisz, E.; Bryant, P.; Balan, S.; Laurine, E.; Tommasi, R.; Singh, R.; Dubey, S.; Peciak, K.; Bird, M.; *et al.* Site-Specific PEGylation at Histidine Tags. *Bioconjug. Chem.* **2012**, *23*, 248–263.
- (15) Casaletto, J. B.; McClatchey, A. I. Spatial Regulation of Receptor Tyrosine Kinases in Development and Cancer. *Nat. Rev. Cancer* **2012**, *12*, 387–400.
- (16) Pasquale, E. B. Eph-Ephrin Bidirectional Signaling in Physiology and Disease. *Cell* **2008**, *133*, 38–52.
- (17) Himanen, J. P.; Yermekbayeva, L.; Janes, P. W.; Walker, J. R.; Xu, K.; Atapattu, L.;



- Rajashankar, K. R.; Mensinga, A.; Lackmann, M.; Nikolov, D. B.; *et al.* Architecture of Eph Receptor Clusters. *Proc. Natl. Acad. Sci. U. S. A.* **2010**, *107*, 10860–10865.
- (18) Wimmer-Kleikamp, S. H.; Janes, P. W.; Squire, A.; Bastiaens, P. I. H.; Lackmann, M. Recruitment of Eph Receptors into Signaling Clusters Does Not Require Ephrin Contact. *J. Cell Biol.* **2004**, *164*, 661–666.
  - (19) Salaita, K.; Nair, P. M.; Petit, R. S.; Neve, R. M.; Das, D.; Gray, J. W.; Groves, J. T. Restriction of Receptor Movement Alters Cellular Response: Physical Force Sensing by EphA2. *Science* **2010**, *327*, 1380–1385.
  - (20) Abulrob, A.; Lu, Z.; Baumann, E.; Vobornik, D.; Taylor, R.; Stanimirovic, D.; Johnston, L. J. Nanoscale Imaging of Epidermal Growth Factor Receptor Clustering: Effects of Inhibitors. *J. Biol. Chem.* **2010**, *285*, 3145–3156.
  - (21) Nimmerjahn, F.; Ravetch, J. V. Fc-Receptors as Regulators of Immunity. *Adv. Immunol.* **2007**, *96*, 179–204.
  - (22) Valentine, R. C.; Green, N. M. Electron Microscopy of an Antibody-Hapten Complex. *J. Mol. Biol.* **1967**, *27*, 615–617.
  - (23) Zhang, X.; Zhang, L.; Tong, H.; Peng, B.; Rames, M. J.; Zhang, S.; Ren, G. 3D Structural Fluctuation of IgG1 Antibody Revealed by Individual Particle Electron Tomography. *Sci. Rep.* **2015**, *5*, 9803.
  - (24) Diebolder, C. a; Beurskens, F. J.; de Jong, R. N.; Koning, R. I.; Strumane, K.; Lindorfer, M. a; Voorhorst, M.; Ugurlar, D.; Rosati, S.; Heck, A. J. R.; *et al.* Complement Is Activated by IgG Hexamers Assembled at the Cell Surface. *Science* **2014**, *343*, 1260–1263.
  - (25) Nguyen, H. H.; Park, J.; Kang, S.; Kim, M. Surface Plasmon Resonance: A Versatile Technique for Biosensor Applications. *Sensors (Switzerland)* **2015**, *15*, 10481–10510.
  - (26) Jones, M. R.; Seeman, N. C.; Mirkin, C. A. Nanomaterials. Programmable Materials and the Nature of the DNA Bond. *Science* **2015**, *347*, 1260901.
  - (27) Jeyachandran, Y. L.; Mielczarski, J. A.; Mielczarski, E.; Rai, B. Efficiency of Blocking of Non-Specific Interaction of Different Proteins by BSA Adsorbed on Hydrophobic and Hydrophilic Surfaces. *J. Colloid Interface Sci.* **2010**, *341*, 136–142.
  - (28) Shaw, A.; Benson, E.; Högberg, B. Purification of Functionalized DNA Origami Nanostructures. *ACS Nano* **2015**, *9*, 4968–4975.
  - (29) Tan, S. C.; Yiap, B. C. DNA, RNA, and Protein Extraction: The Past and the Present. *J. Biomed. Biotechnol.* **2009**, *2009*.
  - (30) Douglas, S. M.; Chou, J. J.; Shih, W. M. DNA-Nanotube-Induced Alignment of Membrane Proteins for NMR Structure Determination. *Proc. Natl. Acad. Sci. U. S. A.* **2007**, *104*, 6644–6648.
  - (31) Stahl, E.; Martin, T. G.; Praetorius, F.; Dietz, H. Facile and Scalable Preparation of Pure and Dense DNA Origami Solutions. *Angew. Chemie - Int. Ed.* **2014**, *53*, 12735–12740.
  - (32) Bellot, G.; McClintock, M. a; Lin, C.; Shih, W. M. Recovery of Intact DNA Nanostructures after Agarose Gel-Based Separation. *Nat. Methods* **2011**, *8*, 192–194.

- (33) Lin, C.; Perrault, S. D.; Kwak, M.; Graf, F.; Shih, W. M. Purification of DNA-Origami Nanostructures by Rate-Zonal Centrifugation. *Nucleic Acids Res.* **2013**, *41*, 1–6.
- (34) Wickham, S. F. J.; Endo, M.; Katsuda, Y.; Hidaka, K.; Bath, J.; Sugiyama, H.; Turberfield, A. J. Direct Observation of Stepwise Movement of a Synthetic Molecular Transporter. *Nat. Nanotechnol.* **2011**, *6*, 166–169.
- (35) Douglas, S. M.; Bachelet, I.; Church, G. M. A Logic-Gated Nanorobot for Targeted Transport of Molecular Payloads. *Science* **2012**, *335*, 831–834.
- (36) Ke, Y.; Bellot, G.; Voigt, N. V.; Fradkov, E.; Shih, W. M. Two Design Strategies for Enhancement of multilayer–DNA-Origami Folding: Underwinding for Specific Intercalator Rescue and Staple-Break Positioning. *Chem. Sci.* **2012**, *3*, 2587.
- (37) Douglas, S. M.; Marblestone, A. H.; Teerapittayanon, S.; Vazquez, A.; Church, G. M.; Shih, W. M. Rapid Prototyping of 3D DNA-Origami Shapes with caDNAno. *Nucleic Acids Res.* **2009**, *37*, 5001–5006.
- (38) Fredriksson, S.; Gullberg, M.; Jarvius, J.; Olsson, C.; Pietras, K.; Gústafsdóttir, S. M.; Ostman, A.; Landegren, U. Protein Detection Using Proximity-Dependent DNA Ligation Assays. *Nat. Biotechnol.* **2002**, *20*, 473–477.
- (39) Macrae, M.; Neve, R. M.; Rodriguez-Viciana, P.; Haqq, C.; Yeh, J.; Chen, C.; Gray, J. W.; McCormick, F. A Conditional Feedback Loop Regulates Ras Activity through EphA2. *Cancer Cell* **2005**, *8*, 111–118.
- (40) Chang, M.; Yang, C. S.; Huang, D. M. Aptamer-Conjugated DNA Icosahedral Nanoparticles as a Carrier of Doxorubicin for Cancer Therapy. *ACS Nano* **2011**, *5*, 6156–6163.